COBEM 2023 27TH INTERNATIONAL CONGRESS OF MECHANICAL ENGENEERING

ABCM Brazilian Society of Mechanical Sciences and Engineering
27th ABCM International Congress of Mechanical Engineering
December 04-08, 2023, Florianópolis-SC, Brazil

COB-2023-1106
EXPLORING INERTIAL AMPLIFICATION MECHANISM IN MONO-COUPLED PERIODIC ROD STRUCTURES

Ms. Gabriel Biancolin Moimás
Dr. Paulo José Paupitz Gonçalves
São Paulo State University – Faculdade de Engenharia de Bauru (FEB), Av. Eng. Luiz Edmundo C. Coube 14-01 - Vargem Limpa - Bauru - SP/SP
gabriel.moimas@unesp.br; paulo.paupitz@unesp.br

Abstract. *The key idea in metamaterials used for vibration control is to achieve frequency ranges where disturbances cannot propagate or are severely attenuated, stopbands or bandgaps. One mechanism to create a bandgap in structure is based on resonant attachment, that creates mechanical filter tuned at a particular frequency range. In this work, longitudinal vibration on a single cell rod structure is investigated in terms of displacement transmissibility. The study is developed by the comparison of a simple rod-spring-rod periodic element with a rod-spring-rod with an inertial amplification mechanism, i. e. a rigid and massless lever, with a concentrated mass in its tip. Considering the oscillations are small the equations of motion of the periodic elements are derived and an analytical solution is obtained in terms of receptance matrix. Results indicate that the inertial amplification mechanism provokes an anti-resonant peak, previously not seen in rod-spring-rod setup, which depends significantly on the lever length and concentrated tip mass. For some relations of lever length and concentrated mass the anti-resonant peak overlaps the transmissibility peak causing a wider bandgap frequency region. Nevertheless, for higher frequencies it is found that the minimum transmissibility remains constant due the inertial force.*

Keywords: *structural vibration, periodic structure, stop bands, inertial amplification mechanism.*

1. INTRODUCTION

Structural vibrations have been frequently studied with the purpose of developing techniques and methodologies for vibration control such as using dynamic absorbers, active control with actuators and sensors and recently with periodic structures. Studys demonstrate that periodic structures, i. e. identical elements connected repeatedly, can reduce vibration in a frequency band in which the elastic waves don't propagate, named stop bands. In the stop band region, the transmissibility and amplitude of vibration is significantly reduced, introducing an effect similar of a filter (MEAD, 1996; HUSSEIN *et al*, 2014).

In order to change the system behavior in terms of transmissibility and amplitude of vibration some components can be introduced in the periodic structures to modify the stop band effect and attenuate peaks at high/low frequency ranges. Studys of Gonçalves *et al.* (2021) and Carneiro *et al.* (2021) indicates that a stiffness adding in periodic elements interferes mainly at low frequencies ranges attenuating the transmissibility peaks and changing lower and upper cut-off frequencies of the stop band. In the other hand, a mass adding in periodic element attenuates the transmissibility peaks and changes considerably the lower and upper cut-off frequencies of the stop band at high frequencies.

Another vibration control device that can be applied is the vibration neutraliser, device consisting of mass and stiffness element tuned to a resonance frequency of the structure. Although of its limitation of acting at one particular resonance frequency, researches to make the vibration neutralisers more robust are being studied, Nehemy *et al.* (2023) developed a passive vibration neutraliser that can adapt automatically to one of two frequencies corresponding to the frequency of an external force.

Similar to vibration neutraliser, the vibration absorbers can also be attached to periodic structures to modify the resonance frequency. Cleante *et al.* (2022) investigate a particular condition where the Bragg and local resonance can be overlapped producing an ultra-wide stop-band in a finite mono-coupled periodic system composed of symmetric cells, demonstrating how to tune the absorber frequency and the influence of damping. In this paper an alternative method using a mechanical inerter applied in a mono-coupled periodic rod system is introduced resulting in an ultra-wide stop-band similar to the effect studied by the mentioned authors.

The inertial adding in periodic elements can be studied by introducing a mechanical inerter in periodic system. The paper of Kuhnert *et al.* (2020) reviews the literature of old and new ideias of inerter introducing some applications of inerter and inerter -like devices, discussing the advantages and disadvantages of using the inerter in vibration isolation in terms of transmissibility and suggesting a strategy of overcome the detrimental effect of inerter at high frequencies.

The concept of inerter was first introduced by Smith (2002), described as a mechanical component equivalent to a capacitor in an electrical circuit, without the restriction of grounding one of its terminals. Since then in literature can be

found many other examples of inerter-like devices: mechanical isolator connected to a duct and vessel containing fluid – hydraulic inertance (GOLDWIN, 1965), lever mechanism capable of converting linear motion into angular motion – dynamic vibration anti-resonant Isolator, named by DAVI (FLANELLY, 1967), redesigned lever type isolator as a pivoted flywheel inerter (JHON & WAGG, 2019), another fluid-based systems as the LIVE (Liquid Inertial Vibration Eliminator) (CRONJÉ *et al*, 2005) and a closed circuit comprising a hydraulic piston (WANG et al. 2011).

The influence of inerter in terms of vibration control of system was extensively studied. In the book of Shearer et al. (1967) the author noted that the mechanical inerter DAVI device causes an anti-resonance in the force or displacement transmissibility, at the expense of degraded high-frequency vibration isolation performance. Depending on mechanical inerter parameters such as lever length and inertia, this antiresonance effect could overlap the resonance of mechanical system providing a wider stop band range. Alujević et al. (2018) investigated the inerter effect in a two-degree-freedom system, concluding that this mechanism enables successful active vibration control for several mechanical systems in addition to improving significantly stability. Chen et al. (2014) carried out the influence of inerter to lower the natural frequencies, demonstrating that the increase of inerter inertia reduces the natural frequencies of multiple degree of freedem systems. Kuznetsov et al. (2011) demonstrated that an improved quarter-car model suspension system with a incorporated inerter can increase passenger comfort, despite of mass of inerter.

In order to investigate the advantages and disadvantages to couple inerter with periodic structure to control vibration, this present work aims to study the structural vibration isolation of a mono-coupled periodic rod structure using a lever mechanism inerter. A comparison to a mono-coupled periodic rod structure without the inerter is also carried out demonstrating that a wider attenuation band occurs depending of lever mechanism inertia parameters despite of a degraded high-frequency vibration isolation performance. Th approach used in this paper is based in the displacement transmissibility of the cell limits and receptance matrix. The expressions derived in this paper can help in the design of the lever mechanism inerter to achieve a wider stop band and a required vibration attenuation.

2. MONO-COUPLED ROD PERIODIC STRUCTURE WITH INERTER

The system discussed here is illustrated in Fig. 1, which consists of a N cell mono-coupled periodic structure. A detail of cell-*n* is comprised of two rods connect by a spring with stiffness s and a lever mechanism. The lever mechanism is a rigid bar articulated in two points which are rigidly connected to rods A and B. At the free tip of the lever, there is a mass *m* that moves according to the relative displacement of the rods causing the mass to rotate at a small angle θ. The two rods are made of the same material, with Young's modulus E, mass density ρ, cross section area A, and length L. F_i and U_i are complex amplitudes of the forces and displacements acting on rods ends. The lever is characterized by two lengths, l_1 is the distance between the two rotating pins, and the total length l_2.

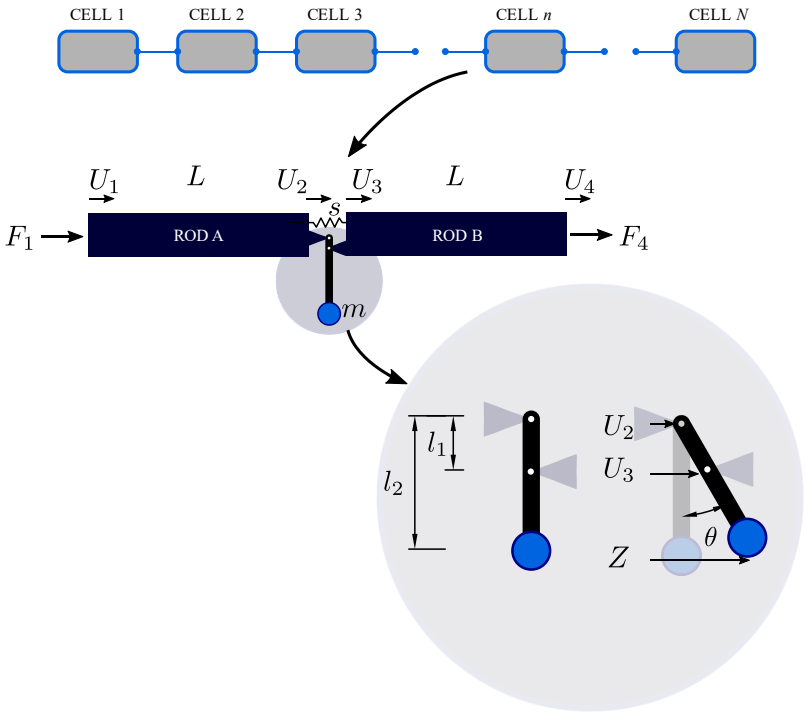

Figure 1. A mono-coupled periodic system with N cells and the detail of a cell consisting of a rod with a spring and lever connection. The zoom gray area shows the lever mechanism.

The periodic system in Figure 1 is a five-degree-of-freedom structure, where Z is the complex displacement of lever mechanism concentrated mass. According to the detail shown in the zoom of the lever mechanism in Fig. 1, the displacements and the angle are related such that

$$\sin(\theta) = \frac{U_2 - U_3}{l_2} = \frac{Z - U_2}{l_1 - l_2} \tag{1}$$

For small displacement amplitudes, i. e. θ, and assuming $\alpha = l_1 / l_2$, it is possible to defined the displacement of the mass at the end of the lever.

$$Z = \alpha U_2 - (\alpha - 1)U_3 \tag{2}$$

To derive the equation of motion described at the system, it's necessary to analyze a single cell and lever mechanisms dynamics through Newton's Second Law. The free body diagram of the rods A and B and lever mechanism can be found in Figure 2.

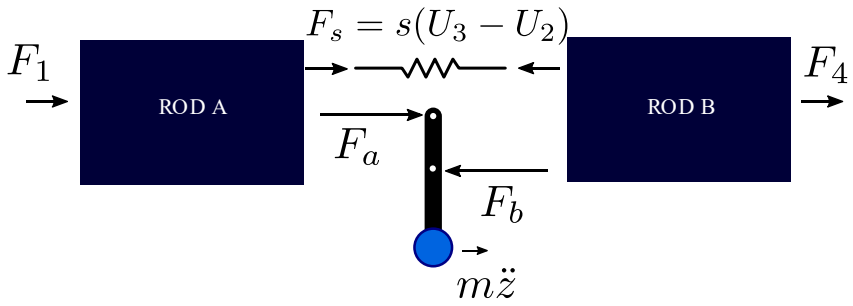

Figure 2. Free body diagram for a cell with internal forces.

Analyzing the free body diagram of lever mechanism, the complex forces acting on the lever and reacting on the rods F_a and F_b can be defined as:

$$\begin{aligned} F_a &= -\omega^2 m\left[\alpha(\alpha-1)U_3 - (\alpha-1)^2 U_2\right] \\ F_b &= -\omega^2 m\left[\alpha^2 U_3 - \alpha(\alpha-1)^2 U_2\right] \end{aligned} \tag{3a,b}$$

The force equilibrium at the four rod ends U_i can be written as:

$$\begin{aligned} &EAU_1' = -F_1 \\ &s\left(U_3 - U_2\right) - EAU_2' = F_a \\ &s\left(U_3 - U_2\right) - EAU_3' = F_b \\ &EAU_4' = F_4 \end{aligned} \tag{4a-d}$$

Where, $U_{\text{ROD A}}(x) = G_1\cos(kx) + G_2\sin(kx)$ and $U_{\text{ROD B}}(x) = G_3\cos(kx) + G_4\sin(kx)$, is a shape function, with constants G_i that satisfies the boundary conditions. The parameter $k = \omega\sqrt{\rho / E}$ is the wavenumber and ω is the circular frequency.

The constants G_i are obtained solving Eq. 4a-d. Therefore, the receptance matrix $\mathbf{R}$, which relates the displacement and the external forces acting on rods ends, can be obtained as:

$$\begin{aligned} &\begin{Bmatrix} U_1 \\ U_4 \end{Bmatrix} = \mathbf{R}\begin{Bmatrix} F_1 / S \\ F_4 / S \end{Bmatrix} \\ &\mathbf{R} = \frac{1}{\Delta}\begin{bmatrix} C_2\cos(2kL) + C_3\sin(2kL) - C_4 & C_1 \\ C_1 & C_2\cos(2kL) + C_3\sin(2kL) + C_4 \end{bmatrix} \end{aligned} \tag{5}$$

Where, $C_1 = \frac{1}{L^2} - \frac{\mu}{\psi}k^2\alpha(\alpha-1)$, $C_2 = \frac{1}{L^2} - \frac{\mu}{\psi}k^2(\alpha^2-\alpha+1/2)$, $C_3 = \frac{k}{2L}\left(-\mu-\frac{1}{\psi}\right)$, $C_4 = \frac{\mu}{\psi}k^2(-\alpha+1/2)$ and $\Delta = \left\{\frac{k}{\psi}\right\}\left\{\frac{k}{2}\left(-\mu-\frac{1}{\psi}\right)\cos(2kL) + \left[\frac{\mu}{\psi}k^2L(\alpha^2-\alpha+1/2) - \frac{1}{L}\right]\sin(2kL) + \frac{k}{2}\left(-\mu+\frac{1}{\psi}\right)\right\}$. In which: stiffness ratio is $\psi = S/(EA/L)$; mass ration is $\mu = m/m_{rod}$,so the rod mass is $m_{rod} = \rho AL$.

The Eq. (5) indicates that the analytical receptance of the periodic structure is not a quite simple expression and it dynamics depends considerably of lever mechanism inertia coefficients: lever ratio α and mass ratio μ, so the lever ratio dependency is greater due being elevated to square. Moreover, the terms of the secondary diagonal of the matrix are equivalent and the terms in the main diagonal of the matrix are different by the opposite signal of C_4, which indicates the reciprocity of the periodic system.

With the receptance matrix in Eq. (5) the displacement transmissibility can be obtained in two different conditions:

a) when there is no force acting in Rod A ($F_1 = 0$)

$$T_A = \frac{U_1}{U_4} = \frac{C_1}{C_2\cos(2kL) + C_3\sin(2kL) + C_4} \tag{6}$$

b) when there is no force acting in Rod B ($F_4 = 0$)

$$T_B = \frac{U_4}{U_1} = \frac{C_1}{C_2\cos(2kL) + C_3\sin(2kL) - C_4} \tag{7}$$

To obtain the influence of the lever mechanism in the dynamics of the studied mono-coupled periodic cell, the equation of motion without the lever mechanism is derived disregarding the forces acting on the lever and reacting on the rods F_a and F_b, so the Eq. 4b and 4c are equal zero. And once again the constants G_i are obtained solving Eq. 4a-d, such that the receptance matrix of the mono-coupled periodic cell without lever mechanism $\left[R_{w,lm}\right]$ can be defined as:

$$\left[R_{w,lm}\right] = \frac{1}{\frac{k}{\psi}\left[-\frac{k}{2\psi}\cos(2kL) - \frac{1}{L}\sin(2kL) + \frac{k}{2\psi}\right]}\begin{bmatrix} \frac{1}{L^2}\cos(2kL) - \frac{k}{2\psi L}\sin(2kL) & \frac{1}{L^2} \\ \frac{1}{L^2} & \frac{1}{L^2}\cos(2kL) - \frac{k}{2\psi L}\sin(2kL) \end{bmatrix} \tag{8}$$

The receptance matrix of the mono-coupled periodic cell without lever mechanism can also be obtained by neglecting the inertia coefficients of lever mechanism in the Δ, C_1, C_2, C_3 and C_4. The non-acting of lever mechanism provides a single expression of the displacement transmissibility, independent of the side of application of external force:

$$T_{A,w,lm} = T_{B,w,lm} = \frac{1}{\cos(2kL) - \frac{EAk}{2s}\sin(2kL)} \tag{9}$$

To provide a factual model a viscous damping is added parallel to the spring, so the dynamic stiffness z of the damper-spring system is given by:

$$z = s + \mathrm{j}\omega c \tag{10}$$

Where: c represents the viscous damping coefficient and j the complex number. The viscous damping coefficient can be related with the rod's parameters such as:

$$c = 2\xi\sqrt{k_{bar}m_{bar}} \tag{11}$$

In which: $k_{bar} = EA/L$ and ξ represents the damping factor, set up underdamped.

The dynamic stiffness of the spring has a real and a complex part, so the stiffness ratio ψ can be divided in a real and complex terms:

$$\psi = \frac{Z}{EA/L} = \frac{s + \mathrm{j}\omega c}{EA/L} = \frac{s}{EA/L} + \mathrm{j}2\xi kL$$

$$\psi = \psi_{Re} + \psi_{Im} j \tag{12}$$

A structural damping is also added to rods by considering the Young Modulus as $E = E_0(1+\mathrm{j}\eta)$, i. e. as an imaginary and real part of E, where E_0 is the Young Modulus of rod material and η is the loss factor. As the longitudinal wave number depends on the Young Modulus, it can be also described, taking into account lower values of η, by imaginary and real components:

$$k = k_{Re} + \mathrm{j}k_{Im} = \omega\sqrt{\frac{\rho}{E_0}}(1 - \mathrm{j}\eta/2) \tag{13}$$

Where the prefix Re and Im indicates the real and imaginary terms, respectively.

In Figure 3, it's seen the T_A behavior in relation to lever ratio α for $\psi = 0.05$, $\mu = 0.05$, $\xi = 0.001$ and $\eta = 0.005$. At the color map the dashed line indicates the anti-resonant magnitude and the yellow color represents the resonant magnitudes. The plots among the color map provides the T_A (blue line) in contrast to the transmissibility of a periodic cell without lever mechanism $T_{A,w,lm}$ (dashed line) for some lever ratios and it's clearly noted the inerter-behavior presented in literature: anti-resonant peak in displacement transmissibility and a degraded high-frequency vibration isolation performance.

Furthermore, when the lever ratio leads to an overlapping of resonant and anti-resonant amplitudes a super attenuation band (SAB) occurs and the anti-resonant has a lower amplitude (SAB 1 and SAB 2 in Figure 3). When the anti-resonant takes place at a different wave number frequency of the resonance, a higher anti-resonant peak comes up, but the SAB doesn't exist (Graphs on left side of Figure 3). The same behavior can be found if we vary the mass ratio μ, despite of a weaker relation in comparison with lever ratio.

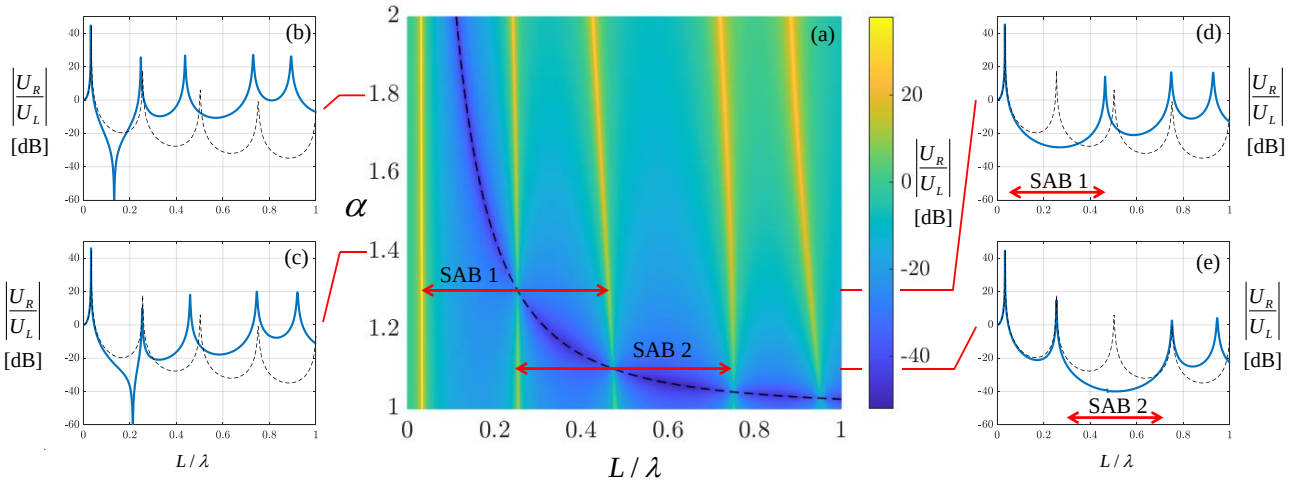

Figure 3. T_A behavior in relation to lever ratio α.

Analyzing the transmissibility expressions, Eq. (6) and (7), it's possible to determine the anti-resonant longitudinal wavenumber (k_{ar}) and the minimum amplitude at higher frequencies. The anti-resonant longitudinal wavenumber can be given by equaling the numerator of Eq. (6) and (7) to zero:

$$k_{ar,T_A} = k_{ar,T_B} = \sqrt{\frac{\psi}{\mu L^2 \alpha(\alpha - 1)}} \tag{14}$$

To obtain the expression for minimum amplitude at higher frequencies, the higher order terms of wavenumber frequency in displacement transmissibility expressions predominate and the others neglected:

$$T_{A,\uparrow k} = \frac{\alpha(\alpha-1)}{(\alpha^2-\alpha+1/2)cos(2kL)+(-\alpha+1/2)}$$
$$T_{B,\uparrow k} = \frac{\alpha(\alpha-1)}{(\alpha^2-\alpha+1/2)cos(2kL)-(-\alpha+1/2)} \quad (15ab)$$

According to Eq. and (15ab) the minimum displacement transmissibility occurs when the denominators must be maximum, i.e. when the $\cos(2kL) = \pm 1$:

$$T_{A,\uparrow k,\min} = T_{B,\uparrow k,\min} = \frac{|1-\alpha|}{\alpha} \quad (16)$$

The Eq. (14) indicates that the anti-resonant wavenumber frequency expression is the same regardless of the side of external force applied, the zoom at the anti-resonant region of Figure 4 confirms it. Equation (16) evidences that the both transmissibility tends to be constant as the longitudinal frequency becomes higher, behavior corroborated with the overlapping of the minimum transmissibility of T_A and T_B and $T_{\uparrow k,min}$ for L/λ greater than 2 in Figure 4.

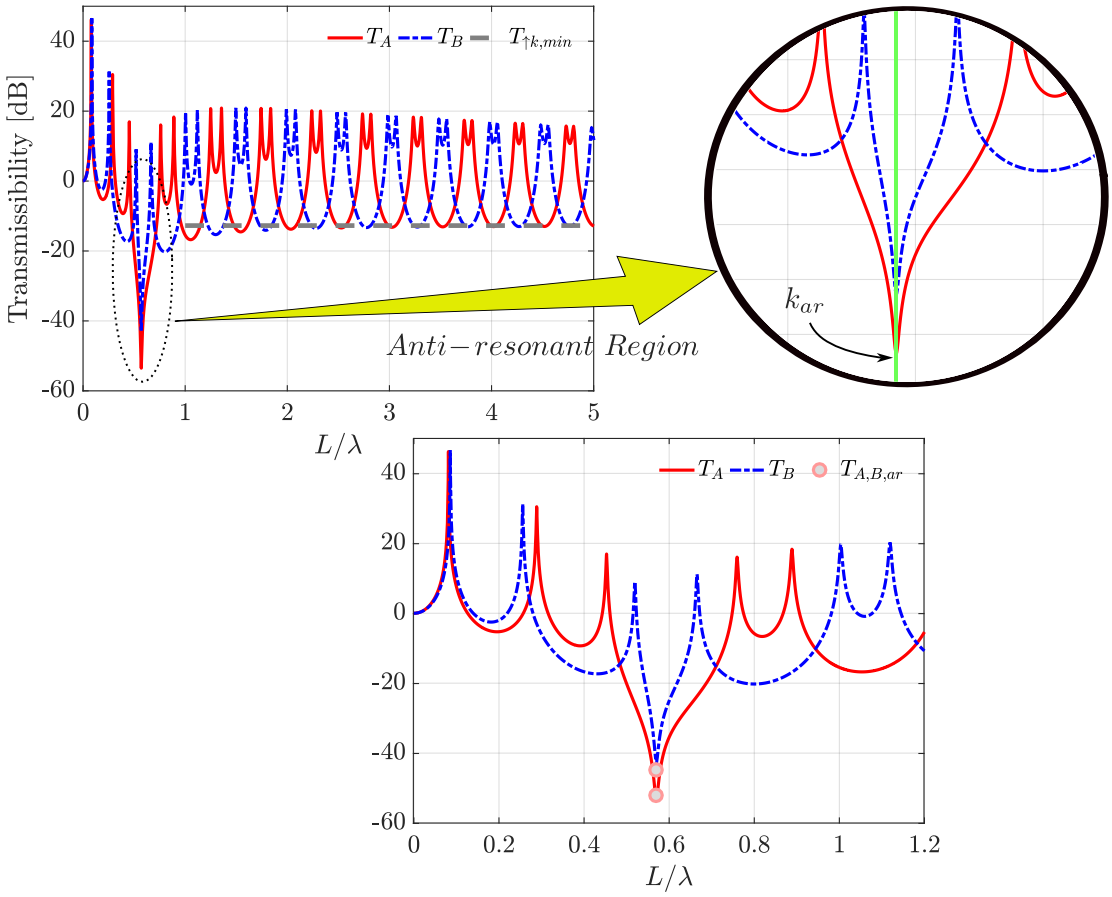

Figure 4. T_A and T_B analysis: comparison, anti-resonant wave number frequency and amplitude. Parameters: $\alpha = 1.3$, $\psi = 0.05$, $\mu = 0.1$, $\xi = 0.0005$ and $\eta = 0.005$.

Due the viscous and structural damping the transmissibility T_A and T_B can be written in real and complex terms, so it's possible to estimate the modulus by the relation $\left|T_{A,B}\right| = \sqrt{T_{Re}{}^2 + T_{Im}{}^2}$. The resulting transmissibility expressions results in a non-trivial expression, however at the anti-resonant amplitude some terms can be neglected, so that at the antiresonance the transmissibility modulus (T_{ar}) can be reduced to:

$$T_{A,ar} = \left| \frac{\dfrac{\psi_{Im}}{2\psi_{Re}L^2}}{C_3 \sin(2kL)} \right|$$

$$T_{B,ar} = \frac{\left| \left(\dfrac{\psi_{Im}}{\psi_{Re}L^2} \right) \right|}{\left\{ \left[C_3 \sin(2kL) \right]^2 + 2C_2C_3 \cos(2kL)\sin(2kL) - 2C_3C_4 \sin(2kL) \right\}^{1/2}} \tag{17ab}$$

In Figure 4, there is a plot of T_A and T_B in comparison for parameters $\alpha = 1.3$, $\psi = 0.05$, $\mu = 0.1$, $\xi = 0.0005$ and $\eta = 0.005$. The antiresonance modulus of transmissibility estimated in Eq. (17ab) are seen in Figure 4. The anti-resonant amplitude of T_A and T_B differs from each other depending on its own resonance longitudinal wavenumber frequencies and the anti-resonant wavenumber frequency caused by lever-mechanism (k_{ar}). When k_{ar} becomes closer to resonance longitudinal wavenumber frequencies, the anti-resonant amplitude becomes lower. This effect can be seen in Figure 4 confronting the displacement transmissibility of T_A and T_B, once k_{ar} is closer to resonance longitudinal wavenumber frequency of T_B, so its amplitude is lower than T_A.

In order to envelope the transmissibility's maximum and minimum, the cosine and sine at the denominator of Eq. (6) and (7) can be written in terms of modulus, i. e. a cosine with a phase, so $C_2 \cos(2kL) + C_3 \sin(2kL) = \left[C_2{}^2 + C_3{}^2 \right]^{1/2} \cos(2kL + \phi)$. Once it's intended to envelope the maximum and minimum the phase can be disregarded, so expanding the cosine in terms of hyperbolic function the simplified transmissibility expressions $T_{A,s}$ and $T_{B,s}$ can be obtained:

$$T_{A,s} = \frac{C_{1,Re}}{\left(C_{2,\mathrm{Re}}{}^2 + C_{3,\mathrm{Re}}{}^2 \right)^{1/2} \left[\cos(2k_{Re}L)\cosh(2k_{Im}L) - j\sinh(2k_{\mathrm{Im}}L)\sin(2k_{Im}L) \right] + C_{4.\mathrm{Re}}}$$

$$T_{B,s} = \frac{C_{1,Re}}{\left(C_{2,\mathrm{Re}}{}^2 + C_{3,\mathrm{Re}}{}^2 \right)^{1/2} \left[\cos(2k_{Re}L)\cosh(2k_{Im}L) - j\sinh(2k_{\mathrm{Im}}L)\sin(2k_{Im}L) \right] - C_{4.\mathrm{Re}}} \tag{18ab}$$

Where: $C_{1,\mathrm{Re}} = \dfrac{1}{L^2} - \dfrac{\mu}{\psi} k_{Re}{}^2 \alpha(\alpha - 1)$, $C_{2,\mathrm{Re}} = \dfrac{1}{L^2} - \dfrac{\mu}{\psi} k_{Re}{}^2 (\alpha^2 - \alpha + 1/2)$, $C_{3,\mathrm{Re}} = \dfrac{k_{Re}}{2L}\left(-\mu - \dfrac{1}{\psi} \right)$,

$C_{4,\mathrm{Re}} = \dfrac{\mu}{\psi} k_{Re}{}^2 (-\alpha + 1/2)$. Considering η is small, the term with real and imaginary k, with exception of cosines and sine functions, can be approximated by it real part, i.e. $k \cong k_{Re}$.

For lower η, $\sin(2k_{Re}L) \ll \cos(2k_{Re}L)$ and at the anti-resonant amplitude $\sinh(2k_{Im}L) \ll \cosh(2k_{Im}L)$ $\sinh(2k_{Im}L) \ll \cosh(2k_{Im}L)$ the line that represents the minimum amplitude (T_{min}) occurs when the denominator is maximum, thus when the term $\cos(2k_{Im}L)$ exists :

$$T_{A,B,\min} = \frac{C_{1,Re}}{\left(C_{2,\mathrm{Re}}{}^2 + C_{3,\mathrm{Re}}{}^2 \right)^{1/2} \cosh(2k_{Im}L) + C_{4.\mathrm{Re}}} \tag{19}$$

To obtain the line that represents the maximum amplitude (T_{max}), the denominator in Eq. (18ab) must be minimum, this occurs when the term $(C_{2,Re}{}^2 + C_{3,Re}{}^2)^{1/2} \cosh(2k_{Im}L) = -C_{4,Re}$. At low wavenumber frequencies, the term $C_{4,Re}$ can

be disregarded due its k^2, in this case the line that represents the maximum amplitude at low wavenumber frequencies ($T_{\downarrow k,max}$) and the expression can be determined only when the term $-jsinh(2k_{Im}L)$ in Eq. (18ab) exists, so:

$$T_{A,B,\max,\downarrow k} = \frac{C_{1,\mathrm{Re}}}{-\left(C_{2,Re}{}^2 + C_{3,Re}{}^2\right)^{1/2} \sinh(2kL)\, j} \tag{20}$$

The maximum and minimum of transmissibility can be seen in Figure 5, in which T_A and T_B are determined for $\alpha = 1.4$, $\psi = 0.05$, $\mu = 0.1$, $\xi = 0.0005$ and $\eta = 0.005$. Clearly, the T_{min} describes the minimum transmissibility regardless of wavenumber longitudinal frequency. Although, the maximum amplitude presents errors as long as the wavenumber frequency increases, as mentioned in text, however about the anti-resonant the maximum amplitude has an accurate prediction.

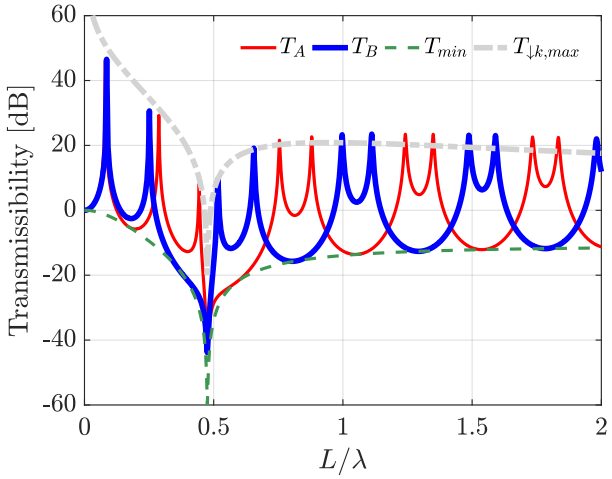

Figure 5. Envelope of maximum and minimum of displacement transmissibility. Parameters: $\alpha = 1.4$, $\psi = 0.05$, $\mu = 0.1$, $\xi = 0.0005$ and $\eta = 0.005$.

3. CONCLUSIONS

The vibration of a mono-coupled rod periodic structure was controlled using a lever mechanism inerter, as described in this paper. The displacement transmissibility showed that the inerter introduced an anti-resonant frequency, which could be used to trigger a wider stop band, depending on the inertial parameters of the lever mechanism, such as the mass ratio and lever ratio. Approximate analytical expressions were derived to obtain the anti-resonant wavenumber frequency and amplitude, minimum and maximum transmissibility.

To illustrate this approach, a lever mechanism with structural and viscous damping was applied to a mono-coupled rod periodic structure. An analytical expression for the anti-resonant frequency and minimum transmissibility amplitude at higher frequencies was determined. The influence of the inertia parameters of the lever mechanism on the transmissibility was evaluated, demonstrating that a super attenuation band occurs when the anti-resonance overlays the resonance peak. By expanding the transmissibility in terms of hyperbolic functions, trivial minimum and maximum lines were derived that envelope the displacement transmissibility.

4. ACKNOWLEDGMENTS

The authors would like to acknowledge São Paulo Research Foundation (FAPESP) grant #2018/15894-0, and The Brazilian Council for Scientific and Technological Development (CNPq) grants 406594/2021-0, 407152/2022-9.

5. REFERENCES

Alujević, N., Čakmak, D., Wolf, H., Jokić, M., 2018. “Passive and active vibration isolation systems using inerter”. *Journal of Sound and Vibration*, Vol. 418, p. 163-183, ISSN 0022-460X.

Carneiro Jr, Brennan, M.J., Gonçalves, P.J.P., Cleante, V.G., Bueno, D.D., Santos, R.B., 2021. "On the attenuation of vibration using a finite periodic array of rods comprised of either symmetric or asymmetric cells", *Journal of Sound and Vibration*, Vol. 511, p. 116217, ISSN 0022-460X.

Chen, M. Z. Q., Hu, Y., Huang, L., Chen, G., 2014. "Influence of inerter on natural frequencies of vibration systems". *Journal of Sound and Vibration*, Vol. 333, Issue 7, p.1874-1887, ISSN 0022-460X.

Cleante, V.G., Brennan, M.J., Gonçalves, P.J.P., Carneiro Jr, J.P., 2022. "On the formation of a super stop-band in finite mono-coupled periodic structures using an array of vibration absorbers: Controlling parameters and physical insight". *Journal of Mechanical Systems and Signal Processing*, Vol. 180, p. 109383, ISSN 0888-3270.

Cronjé, J.M., Heyns, P.S., Theron, N.J., Loveday, P.W., 2005. "Development of a Variable Stiffness and Damping Tunable Vibration Isolator". *Journal of Vibration and Control*, Vol. 11, Issue 3, p. 381-396. doi:10.1177/1077546305048585.

Flanelly, W. G. "Dynamic antiresonant vibration isolator", 1967. Patent, United States Patent and Trademark Office, Registry number: US3322379A, Application date: 03 November 1964, Publication date: 30 May 1967.

Gonçalves, P. J. P., Brennan, M. J., Cleante, V. G., 2021. "Predicting the stop-band behaviour of finite mono-coupled periodic structures from the transmissibility of a single element". *Journal of Mechanical Systems and Signal Processing*, Vol. 154, p. 107512, ISSN 0888-3270.

Goodwin, A., 1965. "Vibration isolators". Patent, United States Patent and Trademark Office, Registry number: US3202388A, Application date: 23 May 1963, Publication date: 24 August 1965.

Hussein, M. I., Leamy, M. J., Ruzzene M., 2014. "Dynamics of Phononic Materials and Structures: Historical Origins, Recent Progress, and Future Outlook". *Applied Mechanics Reviews*, Vol. 66, Issue 4, Article 040802.

John, E.D.A., Wagg, D.J., 2019. "Design and testing of a frictionless mechanical inerter device using living-hinges". *Journal of the Franklin Institute*, Vol. 356, Issue 14, p. 7650-7668, ISSN 0016-0032.

Kuhnert, W. M., Gonçalves, P. J. P., Ledezma-Ramirez, D. F., Brennan, M. J., 2021. "Inerter-like devices used for vibration isolation: A historical perspective. *Journal of the Franklin Institute*, Vol. 358, Issue 1, p. 1070-1086, ISSN 0016-0032.

Kuznetsov, A., Mammadov, M., Sultan, I., Hajilarov, E., 2011. "Optimization of improved suspension system with inerter device of the quarter-car model in vibration analysis". *Archive of Applied Mechanics*, Vol. 81, p. 1427–1437. https://doi.org/10.1007/s00419-010-0492-x

Mead, D.M., 1996. "WAVE PROPAGATION IN CONTINUOUS PERIODIC STRUCTURES: RESEARCH CONTRIBUTIONS FROM SOUTHAMPTON, 1964–1995". *Journal of Sound and Vibration*, Vol. 190, p 495-524, ISSN 0022-460X.

Nehemy, G. F., Rustighi, E., Gonçalves, P.J.P., Brennan, M. J., 2023. "A passive self-tuning vibration neutraliser using nonlinear coupling between the degrees of freedom". *Journal of Mechanical Systems and Signal Processing*, Vol. 185, p. 109786, ISSN 0888-3270.

Shearer, J. L., Murphy, A. T., Richardson, H. H., 1967. *Introduction to system dynamics*. Vol. 44. Addison-Wesley, 1967.

Smith, M. C., 2002."Synthesis of mechanical networks: the inerter," in *IEEE Transactions on Automatic Control*, vol. 47, no. 10, pp. 1648-1662.

Wang, F. C., Hong, M. F., Lin, T. C, 2011. "Designing and testing a hydraulic inerter. Proceedings of the Institution of Mechanical Engineers". *Journal of Mechanical Engineering Science*, Vol. 225, Issue 1, p. 66-72. doi:10.1243/09544062JMES2199.

6. RESPONSIBILITY NOTICE

The authors are the only responsible for the printed material included in this paper.